Catal Lett (2012) 142:771–778
DOI 10.1007/s10562-012-0824-2

Visible-Light-Driven Photodegradation of Rhodamine B on Ag-Modified BiOBr

Lufeng Lu · Liang Kong · Zheng Jiang · Henry H.-C. Lai · Tiancun Xiao · Peter P. Edwards

Received: 22 February 2012 / Accepted: 8 April 2012 / Published online: 4 May 2012

Abstract Ag-modified BiOBr composite photocatalysts were prepared via a simple phase-transfer methodology and used for cleanup of Rhodamine B (RhB) aqueous solution under visible light irradiation. X-ray diffraction, ultraviolet–visible diffuse reflectance spectra (UV–Vis-DRS) and high resolution X-ray photoelectron spectra characterizations confirmed the Ag-modification significantly affected the optical property, structures and reactivity of the BiOBr-based photocatalysts. In the Ag-modification process, a large portion of Ag^{+} may extract Br^{1-} from BiOBr and the as-formed AgBr epitaxially located along the {102} crystal surface of BiOBr. The rest Ag^{+} will be either photo-reduced by methanol into Ag^{0} or form Ag_2O. In nature, the Ag-modified BiOBr materials are multi-junction photocatalysts of $Ag/Ag_2O/AgBr/BiOBr$. The Ag-modification can greatly enhance the absorption of visible light but deteriorates the photocatalytic activity in comparison to the primitive BiOBr in visible-light-driven photodegradation of RhB. The activity of RhB photodegradation on such catalysts is inversely proportional to AgBr loading within 0.2–2.0 wt% region. Such unusual photocatalytic performance was tentatively attributed to the special band structure of the materials.

Keywords Visible light · Photocatalysis · BiOBr · Ag modification · Rhodamine B

L. Lu · L. Kong · Z. Jiang (✉) · H. H.-C. Lai · T. Xiao · P. P. Edwards (✉)
Department of Chemistry, Inorganic Chemistry Laboratory, Oxford OX1 3QR, UK
e-mail: zhjiang76@hotmail.com

P. P. Edwards
e-mail: peter.edwards@chem.ox.ac.uk

Z. Jiang
Jesus College, University of Oxford, Oxford OX1 3DW, UK

Z. Jiang
Environment and Sustainability Institute, University of Exeter, Cornwall Campus, Penryn TR10 9EZ, UK

1 Introduction

The photocatalytic utilization of solar energy on active photocatalysts has drawn considerable interest worldwide because of its great potential for the cleanup environmental contaminations, water splitting, photoreduction of CO_2 and photosensitized polymerizations [1, 2]. In comparison to the extensively studied UV-responsive photocatalysts (TiO_2, ZnO, etc.) which can only harvest a small portion of sunlight (<5 %) due to their wide band gaps, visible-light-responsive photocatalysts may harness more solar energy from the solar spectrum [3, 4]. Great efforts have been made for discovery of new catalytic materials for visible-light-driven photocatalysis [1–8]. Such visible-light-responsive photocatalysts can be pristine photocatalysts with intrinsic narrow bandgap, such as semiconductor compounds of tungsten, molybdenum, bismuth, and metal sulfides, or realized by doping impurity into the UV-responsive photocatalysts [1, 2]. As one of the simplest V-VI-VII bismuth oxyhalides, bismuth oxybromide, BiOBr, has demonstrated high activity and stability in UV–Vis photocatalytic reactions [9–11]. The bandstructure of BiOBr favours to prolong the transfer path of photo-excited electrons and thus reduces the recombination with the photogenerated holes as a result of the unique indirect electron-transition in the band gap region [12]. However, the light absorption of BiOBr is still limited by its relative wide band-gap ($E_g \approx 2.9$ eV) [10].

Doping with nonmetals or transition metals have been extensively adopted to extend the light absorption range of wide bandgap photocatalysts [1–3]. Indeed, iodine-doped BiOBr ($BiOBr_{1-x}I_x$) showed improved visible light adsorption, though their reactivity significantly depends on the I-doping level and the high doping level deteriorated the photocatalytic activity [11, 13]. Surface modification through surface deposition of noble metal or semiconductor represents another effective route to extend the absorption region of the primary photocatalyst. For example, Ag/TiO_2 and AgX/TiO_2 (X = Cl, Br, I) photocatalysts exhibit improved performance with respect to TiO_2 in photocatalysis applications [14]. Metal Ag nano-particles may trap electrons and thus resist the recombination of photogenerated charge carriers, as well as provide visible light response arisen from plasmonic effect of surface nano-Ag [14–16]. AgX may assist photo-generated charge separation as it is supported on other semiconductors [14, 17, 18]. A classic example is $AgBr/TiO_2$, in which AgBr is quite stable despite of its photosensitivity, showing desirable photocatalytic performance under visible light irradiation [14]. Within such kind of hybrid or composite photocatalysts, the interfacial energy bias between the well mixed semiconductors offers additional driving force to suppress recombination of photogenerated charge carries, while the potentials of their conductance band (CB) and valance band (VB) may be tuned to induce targeted reactions.

Ag-modified BiOBr photocatalysts were prepared and employed to photodecompose RhB under visible-light irradiation. XRD, UV–Vis-DRS and XPS were performed to study the structure of the obtained materials and to correlate their photocatalytic reactivity with the structure.

2 Experimental

2.1 Synthesis of BiOBr Support

The BiOBr was prepared using a simple co-precipitation method. Typically, $Bi(NO_3)_3{\cdot}5H_2O$ was dissolved into acetic acid aqueous solution (5 % vol/vol) under vigorous stirring. Yellowish precipitates formed immediately upon adding the aqueous solution containing stoichiometric amount of KBr. After further stirring and aging for 6 h, the precipitate was thoroughly washed and filtered with distilled water. The obtained hydro-gel was then dried under 100 °C to receive BiOBr photocatalyst.

2.2 Modification of BiOBr with Ag

The precipitation-deposition method was used to prepare the Ag/BiOBr catalysts. Typically, 300 mg of BiOBr powder was ultrasonically dispersed into 300 mL of mixed solution of methanol and distilled water (volume ratio of 1:1) prior to adding the appropriate amount of a diluted solution of $AgNO_3$ for producing materials with Ag to BiOBr weight percentages of 0.2, 0.5, 1.0, and 2.0 wt%. The mixture was stirred in the dark for another 60 min before exposure to visible light irradiation for 40 min. The obtained samples were centrifuged and washed with distilled water and 5 mL ethanol before drying. The products were denoted as BiOBr, BiOBr-0.2Ag, BiOBr-0.5Ag, BiOBr-1.0Ag, BiOBr-2.0Ag, which correspond to materials containing 0, 0.2, 0.5, 1.0 and 2.0 wt% Ag, respectively.

2.3 Catalyst Characterization

The bulk and surface characteristics of all samples were investigated by XRD, XPS and UV–Vis-DRS. X-ray powder diffraction (XRD) measurements were carried on a PANalytical X'Pert PRO diffractometer in Bragg–Brentano geometry, using Cu $K\alpha_1$ ($\lambda = 0.15418$ nm) radiation operating under 45 kV and 40 mA, scanning over 5°–60° two-theta. FE-SEM images were obtained on a JSM-6700F field emission scanning electron microscope operated at 10.0 kV. The compositions of the samples were tested by EDAX instrument equipped to JSM-6700F microscope. X-ray photoemission spectra were recorded on a VG ESCALAB 2 XPS spectrometer with an Al Kα monochromatic source and a charge neutralizer. All the binding energies were corrected by referencing C1s peak at 284.5 eV. Core levels of Bi 4*f*, O 1*s*, Br 3*d*, and Ag 3*d* were identified individually. The diffuse reflectance spectra were recorded on a Varian Cary 5000 UV–Vis spectrometer with the scan rate of 300 nm/min.

2.4 Photocatalytic Activity Measurement

The photocatalytic activity of the samples was determined by degradation of Rhodamine B (RhB) in an aqueous solution under visible light irradiation. The optical degradation system consisted of an overhead 300 W Xenon lamp (PLS-SXE300, Beijing Trust Tech) and a UV cutoff filter (UVCUT400, Beijing Trust Tech) to remove UV light. In each experiment, 0.1 g of photocatalyst was dispersed into 100 mL of RhB aqueous solution (20 ppm) in a 500 mL beaker. Prior to irradiation, the beaker was covered by foil and magnetically stirred in the dark for 60 min to establish the adsorption–desorption equilibrium of RhB on the catalyst. During the photocatalytic reaction, approximately 3 mL of suspension was removed by pipette every 5 min and was centrifuged (14,000 rpm, 3 min) to collect the suppressant liquid for sampling. The collected solution was tested by UV–Visible spectroscopy using a Perkin-Elmer Lamda750S UV–visible spectrophotometer. The intensity of the characteristic adsorption peak of RhB at 554 nm was used to determine its degree of degradation. Because the

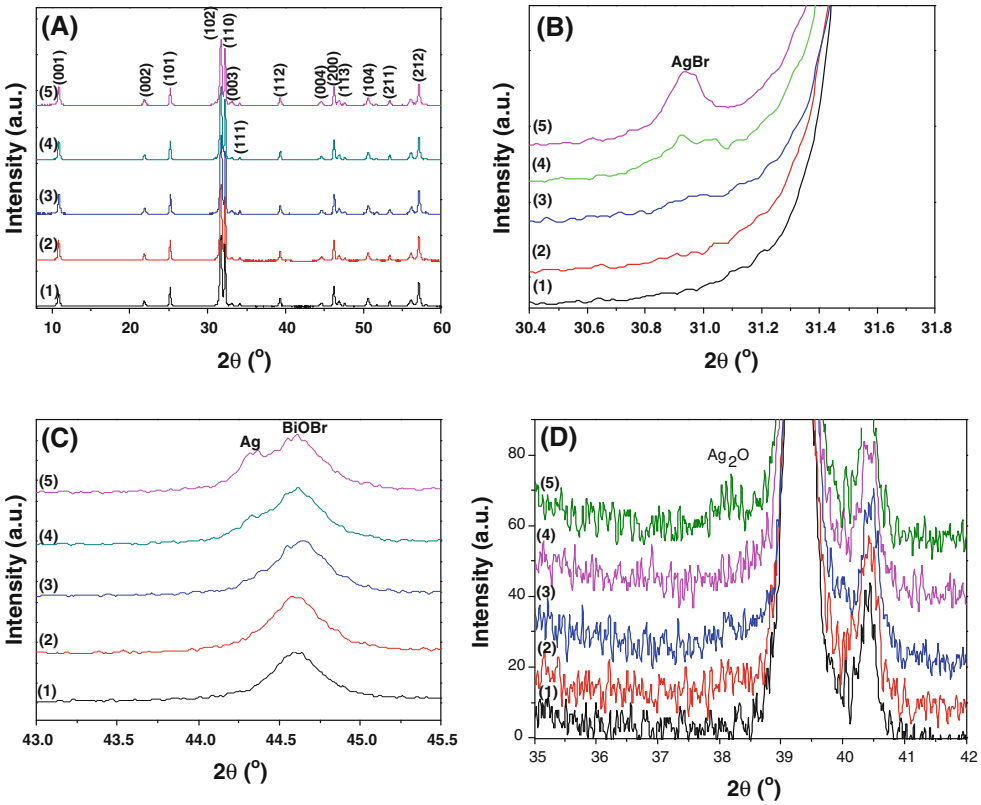

Fig. 1 **a** XRD patterns of the Ag-modified BiOBr, with Miller indices based on the tetragonal cell of BiOBr; (**b**,**c**,**d**) Expansion of diffraction data corresponding to AgBr, Ag and Ag2O. (1)BiOBr, (2)BiOBr-0.2Ag, (3)BiOBr-0.5Ag, (4)BiOBr-1.0Ag, (5)BiOBr-2.0Ag

photocatalysis is following first-order kinetics law, the apparent reaction kinetics constant can be derived from the Arrhenius plots [9].

3 Results and Discussion

3.1 XRD Characterization

Figure 1a presents the XRD patterns for the as-prepared photocatalysts. Only the characteristic Bragg diffraction peaks of tetragonal phase BiOBr (JCPDS 73-2061) were observed in the as-prepared samples with Ag loading less than 0.5 wt%, while the materials with Ag loading greater than 1.0 wt% showed extra Bragg peak of AgBr(JCPDS: 79-0149), which can be well defined to the prominent (002) Bragg diffraction for AgBr of cubic crystal system. No obvious shift associated with BiOBr diffraction peaks was observed in the XRD patterns, suggesting the AgBr or other species were not incorporated into the crystal matrix of the BiOBr. The similar AgBr species were also observed in a Ag/AgBr/BiOBr photocatalysts synthesized using ion-exchange synthesis [19], where only methanol was adopted as solvent for photo-reducing AgBr. Considering the methanol/water mixture involved in our case, the Ag species would be AgBr, Ag or Ag oxides if there were, however, such Ag species are mainly associated with cubic rather than tetragonal crystal system. The mismatch of crystal structure and XRD results excluded the possibility to form AgBr-BiOBr solid solution.

The expansion of the diffraction data in the region of 30° ∼ 31.8° was shown in Fig. 1b, which featured the (002) Bragg diffraction of AgBr at 30.9° and revealed AgBr is the dominant Ag species as its loading greater than 1.0 wt%. It is worthy of noting that the (002) diffraction peak is close to [110] diffraction direction of BiOBr, suggesting AgBr was epitaxially grown along the {110} face of BiOBr. In addition, because there is no extra Br^- was adding with Ag^+ in the preparation process, the appearance of AgBr implies that BiOBr must deviate its stoichiometry in a chemical formula as $BiOBr_{1-x}$, where x is corresponding to the molar Br amount in AgBr. As shown in the extended XRD patterns in Fig. 1c, the small shoulder peaks appear at 44.3° once the Ag loading is greater than 0.5 wt%. The shoulder peaks are associated with (200) diffraction of cubic phased metallic Ag^0 (JCPDS: 893722). The characteristic XRD signal with respect to (011) diffraction of Ag_2O (JCPDS: 722108) was clearly observed in Fig. 1d for 2 wt% Ag loaded sample at 38° but too weak to be identified on other samples because of the limited resolution of XRD in this region. From the afore discussion, it can be concluded the Ag-modified samples are a multi-junction photocatalysts as $Ag/Ag_2O/AgBr/BiOBr$. The existence of Ag and silver oxide may well depict the grey hue of the Ag-modified samples.

Table 1 Crystal parameters of the BiOBr and Ag-modified BiOBr photocatalysts

Samples	Lattice parameters		BiOBr crystallite size (angstrom)	AgBr crystallite size a (angstrom)
	a (angstrom)	c (angstrom)		
BiOBr	3.929	8.121	297	–
BiOBr-0.2Ag	3.926	8.127	250	–
BiOBr-0.5Ag	3.926	8.114	353	5.756
BiOBr-1.0Ag	3.928	8.125	353	5.765
BiOBr-2.0Ag	3.927	8.124	354	5.779

The diffraction intensity of AgBr was found to increase as Ag loading increase, suggesting that the AgBr crystallites became larger at Ag loading of 1.0 wt% or greater. The crystallite sizes of BiOBr in the Ag-modified materials were calculated from the half maximum full width of the (102) Bragg peak, using the Scherrer equation, and reported in Table 1. With a slight expansion of the unit cell, the lattice parameters of BiOBr species in the Ag-modified samples are almost similar to those of pure BiOBr (a = 3.923(5)Å, c = 8.105(2)Å) [10]. However, except for BiOBr-0.2Ag, the BiOBr crystallite sizes of the Ag-modified BiOBr materials are slightly larger than the unadulterated BiOBr. In addition, the crystallite sizes of AgBr were also increased as more Ag loaded as listed in Table 1.

3.2 SEM Images of the Ag-Modified BiOBr

The typical SEM images of as-prepared BiOBr and a typical Ag-modified BiOBr samples are shown in Fig. 2. The obtained samples were flake-like powders with average diameter of approximately 300 nm and a thickness about 40 nm. The morphology of the Ag-modified BiOBr looks the same as that of pure BiOBr. Because of the low resolution of the SEM in use,it is difficult to distinguish Ag species from the BiOBr through SEM images or the energy dispersive X-ray spectroscopy (EDS) of the BiOBr flakes despite that the Ag can be determined from the EDS spectra.

3.3 UV–Vis-DRS of Ag-Modified BiOBr

Figure 3a shows the UV–Vis adsorption spectra derived from the diffuse reflectance spectra (UV–Vis DRS) of the Ag-modified BiOBr samples. All the samples may absorb light over 420 nm in the visible-light region. In comparison with the unadulterated BiOBr sample, the Ag-modification significantly extended the light absorption to a much broader visible-light region from 425 to 800 nm. The enhanced light absorption of Ag-modified samples, particularly in the 450–800 nm region, highly depends on the Ag loading amount. These results are consistent with the pale yellow appearance of unadulterated BiOBr and the grey appearance of the Ag-modified BiOBr materials, suggesting new species, Ag and Ag_2O, were generated during the Ag modification process.

The corresponding band gap energies (E_g) of Ag-modified BiOBr, derived from the formula $E_g = 1239.8/\lambda_g$ [10], are listed in Table 2. The E_g of the samples falls in 2.71–2.84 eV range, depending on Ag loading amount. The steep drop of the reflectance spectra of the composite photocatalysts were typical absorption induced by band gap transition rather than transitions from impurity levels which were featured with tailed absorption spectra [20]. The improved visible-light absorption in the 425–800 nm can be attributed to the contributions of Ag modification. Similar phenomena were reported for AgBr–Ag–Bi_2WO_6 and Ag–AgBr/BiOBr, where the enhanced absorptions

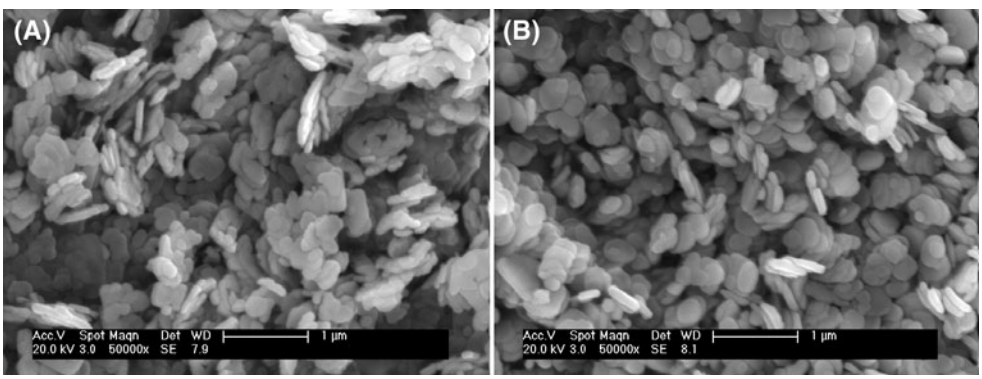

Fig. 2 The FE-SEM images of Ag-modified BiOBr samples: BiOBr(**a**) and BiOBr-Ag1.0 wt%(**b**)

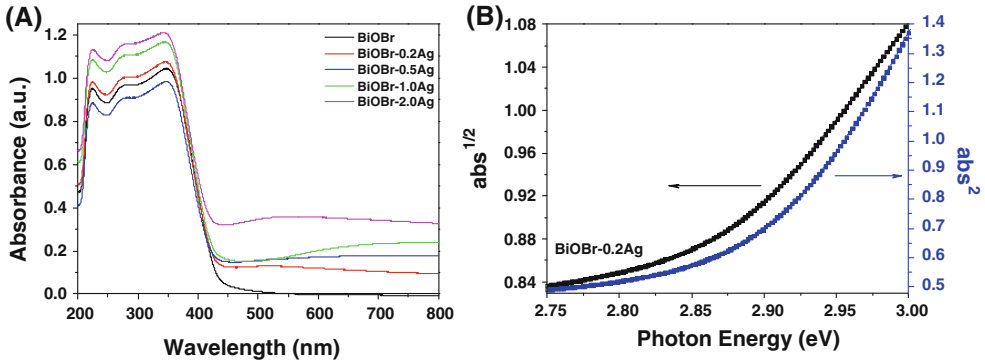

Fig. 3 UV-Vis spectra of the Ag-modified BiOBr samples (**a**) and the optical transition property of the BiOBr-0.5Ag sample (**b**)

Table 2 The optical properties and apparent reaction rate constants of the Ag-modified BiOBr

Sample	BiOBr	BiOBr-0.2Ag	BiOBr-0.5Ag	BiOBr-1.0Ag	BiOBr-2.0Ag	P25 TiO_2
λ_{edge} (nm)	438	442	444	450	457	386
Band gap (eV)[a]	2.83	2.81	2.79	2.76	2.71	3.21
k ($g^{-1}min^{-1}$)[b]	0.231	0.2	0.179	0.14	0.093	0.014

Note: [a]the bandgap was calculated via $Eg = 1240/\lambda_{edge}$; [b]apparent reaction rate constant was derived from Arrhenius plot

were attributed to the plasmonic effects of nano-scaled Ag [16, 19]. In our Ag-modified BiOBr samples, the plasmonic effect arisen from nano-Ag^0 can also be observed within 500–600 nm wavelength region; however, the contributions from Ag_2O and Ag cannot be excluded and must be accounted.

The electron transition characteristics (direct or indirect) of the photocatalysts were analyzed by processing the sharp absorption edge according to the equation: $\alpha \cdot hv = A(hv - E_g)^{n/2}$; where α, v, E_g and A are absorption coefficient, light frequency, band gap, and a constant, respectively. Among them, n is determined by the type of optical transition of a semiconductor [20]. For a specific semiconductor, the absorption coefficient is linear with $(hv - E_g)^2$ (n = 4) for direct transitions in the absorption edge region, but linear with $(hv - E_g)^{1/2}$ (n = 1) for indirect transitions. The band gap energy (E_g) of the Ag-modified BiOBr can thus be estimated from the data plot of $(\alpha \cdot hv)^{1/2}$ and $(\alpha \cdot hv)^2$ versus photon energy (hv), respectively [21, 22]. Figure 3b shows the transition plots of BiOBr-0.5Ag, where the nonlinear plots of $(\alpha \cdot hv)^{n/2}$ versus hv indicate that the composite samples are not indirect or direct semiconductors. The unusual transition feature of the Ag-modified samples can be reasonably attributed to the band structure changes of the samples induced by Ag-species on the surface of BiOBr.

3.4 XPS Analysis of the Ag-Modified BiOBr

The surface element composition and oxidation state of the Ag-modified BiOBr samples were identified by high-resolution X-ray photoelectron spectroscopy (XPS). The chemical shifts of the binding energy arising from the surface charging effect were calibrated from the binding energy (B.E) of adventitious surface C 1s at 284.5 eV. Figure 4a shows the Ag 3d spectra of three Ag-modified BiOBr samples. The two broad XPS peaks are corresponding to $3d_{3/2}$ and $3d_{5/2}$ spectra of Ag [23, 24], respectively. The deconvoluted Ag XPS spectra show that Ag^+ and Ag^0 species are co-existing in the samples. The fitted peaks at 368.2 and 374 eV can be attributed to $3d_{3/2}$ and $3d_{5/2}$ spectra of Ag^0, which is the dominant Ag species. The peaks with BE centered at 369 eV and 375 eV are due to $3d_{5/2}$ and $3d_{3/2}$ core lines of Ag^+ in AgBr [25, 26]. The presence of Ag_2O may also be confirmed by the shoulders with B.E. at 369.4 ($3d_{5/2}$) and 375.5 eV ($3d_{3/2}$), which depicted the surface grey hue of the Ag-modified samples. The intensity of the Ag XPS spectra increased as increasing the Ag loading amount. It is worth noting that the peak areas of Ag^0, corresponding to its molar ratio, increased more significantly than those of Ag^+, revealing the effective reduction of Ag^+ upon the Ag-modification via of photo-deposition [14, 16]. However, under the photo-deposition treatment, it cannot completely remove the soluble oxygen and hydroxyl group of H_2O, which would facilitate Ag^+ to form Ag_2O.

Figure 4b compares the Bi 4f spectra Ag-modified BiOBr samples with AgBr loadings of 0.2, 0.5, and 1.0 wt%. The strong peaks at 165 and 160 eV were characteristic core line of Bi $4f_{5/2}$ and Bi $4f_{7/2}$ in BiOBr. As AgBr loading increased from 0.2 to 1.0 wt%, the Bi $4f_{5/2}$ and $4f_{7/2}$ peaks show slight blue shifts which should be

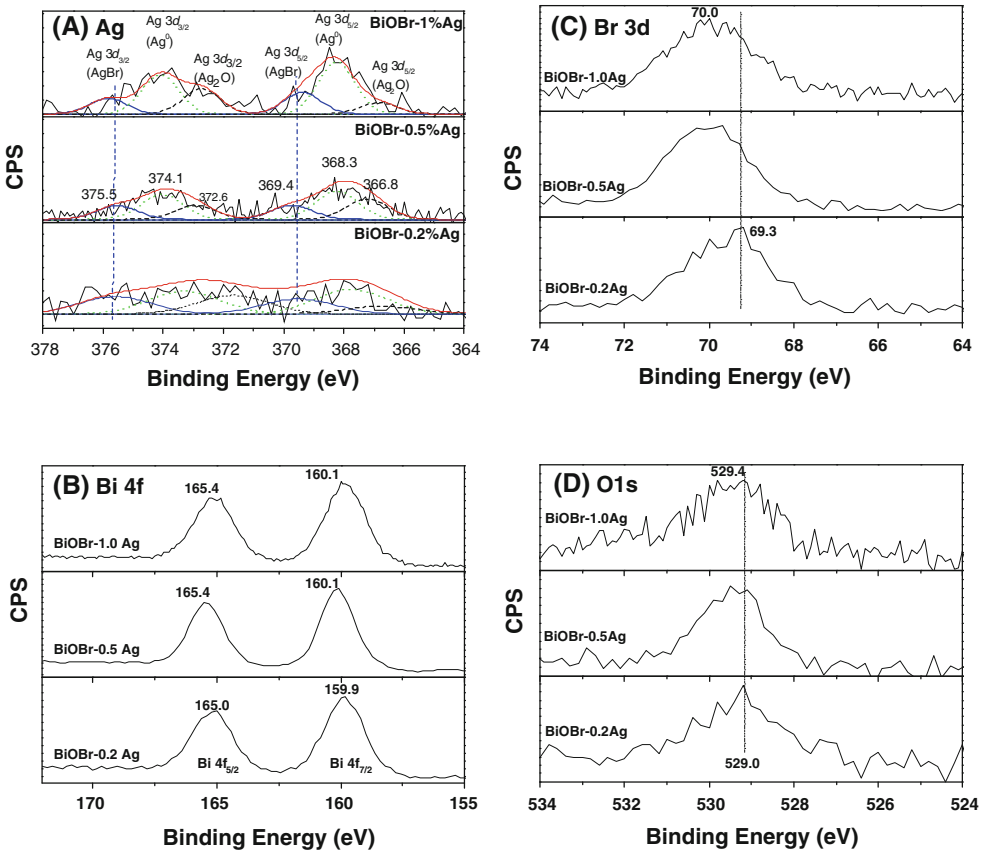

Fig. 4 The X-ray photoelectron spectra of: (**a**) Ag 3*d*, (**b**) Bi 4*f*, (**c**) Br 3*d* and (**d**) O 1*s*

induced by Ag-modification. Figure 4c shows the XPS spectra of Br 3*d*, where the B.E. around 68 eV can be attributed to the Br^{-1} in the BiOBr and AgBr. As Ag-loading increased, the binding energy of Br^{-} is also bule shited [27]. Figure 4d shows the broad symmetric O 1*s* XPS spectra, which are assigned to O^{2-} in BiOBr and remains unchanged in comparison to that in BiOBr [28]. The B.E. shifts for Ag and Br in the Ag(0.2 wt%)-modified BiOBr sample were thought to arise from the lower electronegativity of Ag (1.93) with respect to Bi (2.02), which produces weaker chemical binding in the Ag–Br bond compared to the Bi–Br bond. The changes of binding energy for elements indicate there are strong interactions between them, and these interactions are dependent on Ag loading. The XPS results further confirmed the multi-junction nature of the Ag-modified BiOBr photocatalysts.

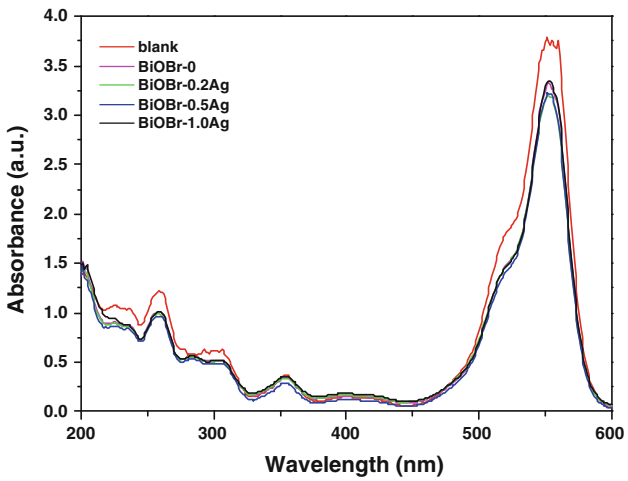

Fig. 5 UV-vis spectra of the RhB solution upon establishment of the adsorption–desorption equilibrium

3.5 Photocatalytic Activity

Surface adsorption of the dye is the key step for photocatalytic reaction and plays important roles in determining photocatalytic degradation activity [10]. Figure 5 shows the light absorption spectra of the RhB solution after the adsorption–desorption equilibrium established. It can be seen that all the samples have almost the same absorption spectra regardless of the Ag-modification, implying that Ag-modification does not significantly affect the surface adsorption capacity of RhB on BiOBr.

The activity of the RhB photodegradation on the Ag-modified BiOBr samples can be compared through the variation of characteristic RhB absorption band at 554 nm under visible-light irradiation [29]. As shown in Fig. 6a, without catalyst, the concentration of RhB remains unchanged under the visible-light irradiation, while RhB

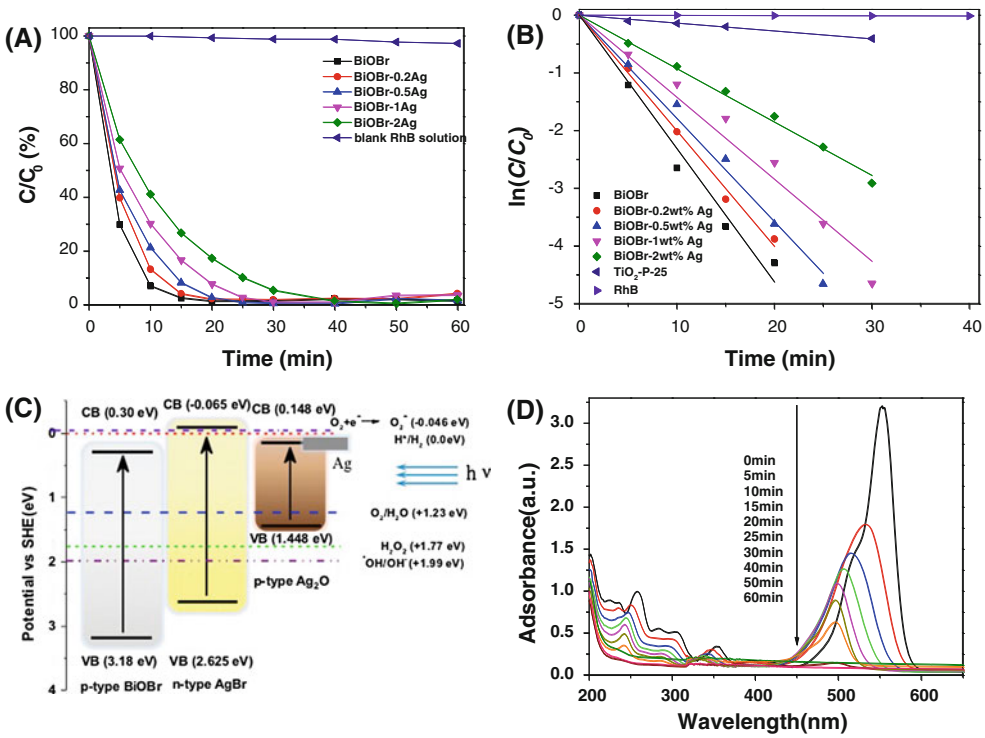

Fig. 6 The photodegradation activity (**a**) and Arrhenius plots (**b**) of RhB photodegradation on the Ag-modified BiOBr samples; schematic diagram of band structure of the Ag-modified BiOBr (**c**); the time-dependence spectra of the RhB solution upon its photodegradation on the BiOBr-0.2 wt% Ag (**d**)

may be completely decomposed in 40 min over BiOBr and Ag-modified BiOBr catalysts. The derived Arrhenius plots of the RhB decomposition on the catalysts were shown in Fig. 6b and the derived rate constants of corresponding catalysts, *k*, were listed in Table 2. The results indicated the photocatalytic performance of the as-prepared modified catalysts is significantly dependent on the Ag loading and their RhB photodegradation activity declined with Ag loading in the following order: BiOBr > BiOBr-0.2Ag > BiOBr-0.5Ag > BiOBr-1.0Ag > BiOBr-2.0Ag. The activity results suggest that Ag-modification of BiOBr through the current methodology deteriorates the photocatalytic activity. This degraded activity maybe arises from the formation of Ag_2O via photodegradation of AgBr on the surface of BiOBr.

Figure 6c presents the schematic band structures of the hybrid photocatalysts of the Ag-modified BiOBr. Although the AgBr and BiOBr may form heterojunction structure which facilitates the separation of photogenerated charge carriers, the surface Ag_2O would mask the reactive sites of AgBr and BiOBr, as well as block the incident radiation onto the reactive species, namely prevent the generation of charge carries. Ag_2O has more positive conductance band and more negative valance band than those of AgBr and BiOBr, suggesting it has weaker reduction and oxidation ability in photocatalytic reaction. It was well documented the nano-scaled Ag particles on the catalysts surfaces would contribute a lot on photocatalysis, particularly the plasmonic effects [14, 16, 19], however, the work function of Ag^0 localizes on the CB close to the standard potential of hydrogen, which cannot improve the photoactivity of the Ag-modified BiOBr samples or cannot compensate the negative contribution from the trace amount of Ag_2O. In addition, the formation of AgBr withdraws Br from BiOBr, which deformed the BiOBr to generated surface defects and the defects might serve the recombination centers of the photogenerated charge carriers as a result of decreased reactivity of the Ag-modified BiOBr samples.

It is worthy of noting that the RhB decomposition is a gradual progress, which is much different from the photocatalytic decomposition of methylene blue (MB) over TiO_2 based semiconductors [6, 7]. Figure 6d shows the absorption spectra variation of RhB versus irradiation time for AgBr (0.2 wt%)–BiOBr. The characteristic absorption band of RhB at 554 nm diminished quickly, accompanied by a slight concomitant red-shift from 554 to 492 nm of the maximum absorption. This phenomenon may be interpreted as the light absorption of the incomplete mineralized intermediates of RhB during the irradiation process.

4 Conclusion

Ag-modified BiOBr samples have been prepared via a two-step precipitation-photodeposition method. The Ag species in the catalysts are mainly AgBr and the small amounts of Ag and Ag_2O. The Ag-modification significantly enhances the visible-light absorption, particularly in the range of 430–800 nm, however, it decreases the photocatalytic

activity of the modified catalysts in RhB photodegradation with respect to the pure BiOBr. The decreased activity is thought to arise from the formation of Ag_2O on the surface of BiOBr, which mask the reactive sites of either AgBr or BiOBr and block incident radiation. The removal of Br^- from BiOBr to form AgBr will create surface defects of BiOBr, which negatively affect the separation of the photogenerated electron/hole.

Acknowledgments This work was financially supported by the principal's major fund at Jesus College, University of Oxford, Oxford Challenge Seed Fund and UK Photocatalysis Network. Jiang appreciates Sir John Houghton Fellowship at Jesus College (Oxford), Shell Foundation, and the grants of Royal Society (TG092414 and TG101750). Lufeng thanks the financial support from Sinopec, China.

References

1. Pan JH, Dou H, Xiong Z, Xu C, Ma J, Zhao XS (2010) Porous photocatalysts for advanced water purifications. J Mater Chem 20:4512–4528
2. Jiang Z, Xiao T, Kuznetsov VL, Edwards PP (2010) Turning carbon dioxide into fuel. Philos Trans R Soc A 368:3343–3364
3. Han F, Kambala VSR, Srinivasan M, Rajarathnam D, Naidu R (2009) Tailored titanium dioxide photocatalysts for the degradation of organic dyes in wastewater treatment: a review. Appl Catal A 359:25–40
4. Hernandez-Alonso MD, Fresno F, Suarez S, Coronado JM (2009) Development of alternative photocatalysts to TiO_2: challenges and opportunities. Energy Environ Sci 2:1231–1257
5. Kou JH, Gao J, Li ZS, Zou ZG (2010) Research on photocatalytic degradation properties of organics with different new photocatalysts. Curr Org Chem 14:728–744
6. Jiang Z, Al-Shahrani F, Lin T-W, Cui Y, Xiao T (2007) Visible light activated mesoporous TiO_2–xNx nanocrystalline photocatalyst. In: Dongyuan Zhao SQYT, Chengzhong Y (eds) Studies in surface science and catalysis, vol 165. Elsevier, Amsterdam, pp 355–359
7. Jiang Z, Yang F, Luo N, Chu BTT, Sun D, Shi H, Xiao T, Edwards PP (2008) Solvothermal synthesis of N-doped TiO_2 nanotubes for visible-light-responsive photocatalysis. Chem Commun 1(47):6372–6374
8. Luo N, Jiang Z, Shi H, Cao F, Xiao T, Edwards PP (2009) Photocatalytic conversion of oxygenated hydrocarbons to hydrogen over heteroatom-doped TiO_2 catalysts. Int J Hydrogen Energy 34:125–129
9. Kong L, Jiang Z, Xiao T, Lu L, Jones MO, Edwards PP (2011) Exceptional visible-light-driven photocatalytic activity over BiOBr–$ZnFe_2O_4$ heterojunctions. Chem Commun 47:5512–5514
10. Jiang Z, Yang F, Yang G, Kong L, Jones MO, Xiao T, Edwards PP (2010) The hydrothermal synthesis of BiOBr flakes for visible-light-responsive photocatalytic degradation of methyl orange. J Photochem Photobiol A Chem 212:8–13
11. Wang W, Huang F, Lin X, Yang J (2008) Visible-light-responsive photocatalysts xBiOBr–(1 − x)BiOI. Catal Commun 9:8–12
12. Huang WL, Zhu Q (2009) Structural and electronic properties of BiOX (X = F, Cl, Br, I) considering Bi 5f states. Comput Mater Sci 46:1076–1084
13. Jia Z, Wang F, Xin F, Zhang B (2011) Simple solvothermal routes to synthesize 3D $BiOBr_xI_{1-x}$ microspheres and their visible-light-induced photocatalytic properties. Ind Eng Chem Res 50:6688–6694
14. Hu C, Lan Y, Qu J, Hu X, Wang A (2006) Ag/AgBr/TiO_2 visible light photocatalyst for destruction of azodyes and bacteria. J Phys Chem B 110:4066–4072
15. Herrmann J-M, Tahiri H, Ait-Ichou Y, Lassaletta G, González-Elipe AR, Fernández A (1997) Characterization and photocatalytic activity in aqueous medium of TiO_2 and Ag-TiO_2 coatings on quartz. Appl Catal B 13:219–228
16. Zhang L, Wong K-H, Chen Z, Yu JC, Zhao J (2009) AgBr–Ag–Bi_2WO_6 nanojunction system: a novel and efficient photocatalyst with double visible-light active components. Appl Catal A Gen 363:221–229
17. Wang P, Huang B, Zhang Q, Zhang X, Qin X, Dai Y, Zhan J, Yu J, Liu H, Lou Z (2010) Highly efficient visible light plasmonic photocatalyst Ag@AgBr. Chem A Eur J 15:1821–1824
18. Cheng H, Huang B, Dai Y, Qin X, Zhang X (2010) One-step synthesis of the nanostructured AgI/BiOI composites with highly enhanced visible-light photocatalytic performances. Langmuir 26:6618–6624
19. Cheng H, Huang B, Wang P, Wang Z, Lou Z, Wang J, Qin X, Zhang X, Dai Y (2011) In situ ion exchange synthesis of the novel Ag/AgBr/BiOBr hybrid with highly efficient decontamination of pollutants. Chem Commun 47(25):7054–7056
20. Butler MA (1977) Photoelectrolysis and physical properties of the semiconducting electrode WO_2. J Appl Phys 48(5):1914–1920
21. Tang J, Ye J (2005) Photocatalytic and photophysical properties of visible-light-driven photocatalyst $ZnBi_{12}O_{20}$. Chem Phys Lett 410:104–107
22. Zhang K-L, Liu C-M, Huang F-Q, Zheng C, Wang W-D (2006) Study of the electronic structure and photocatalytic activity of the BiOCl photocatalyst. Appl Catal B 68:125–129
23. Tian G, Chen Y, Bao H-L, Meng X, Pan K, Zhou W, Tian C, Wang J-Q, Fu H (2012) Controlled synthesis of thorny anatase TiO_2 tubes for construction of Ag–AgBr/TiO_2 composites as highly efficient simulated solar-light photocatalyst. J Mater Chem 22(5):2081–2088
24. Strydom CA, Van Staden JF, Strydom HJ (1991) An XPS investigation of silver bromide-coated ion-selective electrodes. Electroanalysis 3:815–821
25. Tjeng LH, Meinders MBJ, van Elp J, Ghijsen J, Sawatzky GA, Johnson RL (1990) Electronic structure of Ag_2O. Phys Rev B 41:3190–3199
26. Kaushik VK (1991) XPS core level spectra and Auger parameters for some silver compounds. J Electron Spectrosc Relat Phenom 56:273–277
27. Moulder JF, Stickle WF, Sobol PE, Bomben KD (1992) Handbook of X-ray photoelectron spectroscopy. Perkin Elmer Corporation Physical Electronics Division, Eden Prairie
28. Dharmadhikari VS, Sainkar SR, Badrinarayan S, Goswami A (1982) Characterisation of thin films of bismuth oxide by X-ray photoelectron spectroscopy. J Electron Spectrosc Relat Phenom 25:181–189
29. Yu K, Yang S, He H, Sun C, Gu C, Ju Y (2009) Visible light-driven photocatalytic degradation of Rhodamine B over $NaBiO_3$: pathways and mechanism. J Phys Chem A 113:10024–10032